

Geometric constraints for building reconstruction from InSAR data of urban areas

U. Stilla, U. Sörgel, U. Thönnessen

FGAN-FOM Research Institute for Optronics and Pattern Recognition, Gutleuthausstr. 1, 76275 Ettlingen, Germany

email: {usti, soe}@fom.fgan.de

ABSTRACT

The automatic 3-D reconstruction of buildings for the generation of city models is of great interest for different tasks. Besides the classical photogrammetric approaches to determine object heights indirectly, range sensors like laser (LIDAR) and interferometric SAR (InSAR) play an important role since recent years. From both sensors images are produced with a ground resolution better than a meter. In this paper we focus on the analysis of InSAR data for the reconstruction of buildings in dense built-up areas. The data acquisition and the special properties of the InSAR principle are briefly described. A segmentation approach for building reconstruction is proposed. For the analysis of InSAR special effects are taken into account, which are caused by the side-looking illumination. The estimation of the signal noise is considered in the segmentation process. Besides the elevation, the intensity information is exploited to detect building areas. The results show that building reconstruction is possible from InSAR, but the achievable level of detail cannot be compared with LIDAR. Inherent geometric constraints which limit the reconstruction of buildings from SAR data of dense urban areas are discussed. A simulation of geometric effects in SAR images based on LIDAR data is carried out. This may be used for assessing different situations of data acquisition and mission planning.

Keywords: building reconstruction, InSAR, dense built-up areas

1. Introduction

Three-dimensional city models are of great interest for visualization, simulation and monitoring purposes in different fields. A typical application is the visualization of the influence of a planned building to the surrounding townscape for city and regional planning. Additionally, there is a growing demand for such models in civil and military mission planning. City models are used as basis for simulation e.g. in the fields of environmental engineering for microclimate investigations or telecommunications for transmitter placement. Furthermore, 3D information can be used for monitoring, e.g. damage assessment after an earth quake. All the mentioned tasks require knowledge about the 3D structure of buildings. Besides the classical photogrammetric approaches to determine object heights indirectly, range sensors like LIDAR and interferometric SAR (InSAR) play an important role since recent years.

For topographic mapping data acquisition in nadir view is advantageous, especially in dense urban scenes with elevated objects. The LIDAR principle allows airborne applications in oblique (e.g. obstacle warning systems [Armbruster & Bers, 1998]) and in nadir view (e.g. building reconstruction [Stilla & Jurkiewicz, 1999]) as well. In contrast to LIDAR the SAR principle requires a side-looking illumination. LIDAR systems for surveying approaches base on the time-of-flight measurement of reflected infrared laser pulses, while InSAR exploits the phase difference of two measurements of the radar cross-section. Current laser systems achieve a higher accuracy compared to radar systems which are more sensitive to noise, because the measurement is based on a phase difference of two signals. Typically, the obtained accuracy is in the order of decimeter for LIDAR and about some meter for InSAR. LIDAR and InSAR are both active systems which illuminate the scene with electromagnetic waves and measure the backscattered signal component. Due to the different wavelengths (e.g. LIDAR: 1.5 μm , SAR: 3cm) special surface properties are sensed, because the reflectance depends on the surface roughness compared to the wavelength. Furthermore, different behavior concerning atmospheric attenuation and weather conditions are observed. While radar shows almost no sensitivity to weather influence, laser is attenuated from rain or fog and the signal might be reflected away from the sensor if the surface is covered with frost or ice. Another advantage of SAR is the opportunity to record large areas in a short time and from a large distance.

Due to the mentioned features, both sensors are of interest for the generation of 3D descriptions [Gamba & Houshmand, 2000]. For some applications, e.g. disaster management LIDAR data [Kakumoto et al., 1997] as well as InSAR data [Takeuchi et al., 2000] were evaluated. A fusion of LIDAR and InSAR data of vegetated areas was proposed by Slatton et al. [2000]. The fusion of large scale data taken from elevated man-made objects in dense built-up areas is more difficult. This is caused by special geometric and distortions of InSAR data. Such distortions are e.g. the interference of large parts of

the mapped scene by dominant scatters and the deviation of the elevation measurements due to system noise. Furthermore, the SNR varies remarkably in the scene depending on the surface properties.

A crucial step for the generation of 3D-vector descriptions of buildings from InSAR is the segmentation of the elevation data. Recently, approaches for building reconstruction in InSAR elevation data were proposed, which either apply model-based machine-vision methods [Gamba & Houshmand, 2000] or take typical phenomena into account [Bolter & Leberl, 2000], [Leberl & Bolter, 2001]. In this paper we focus on the acquisition and segmentation of InSAR data for the reconstruction of buildings, with emphasis on the sensor properties of SAR.

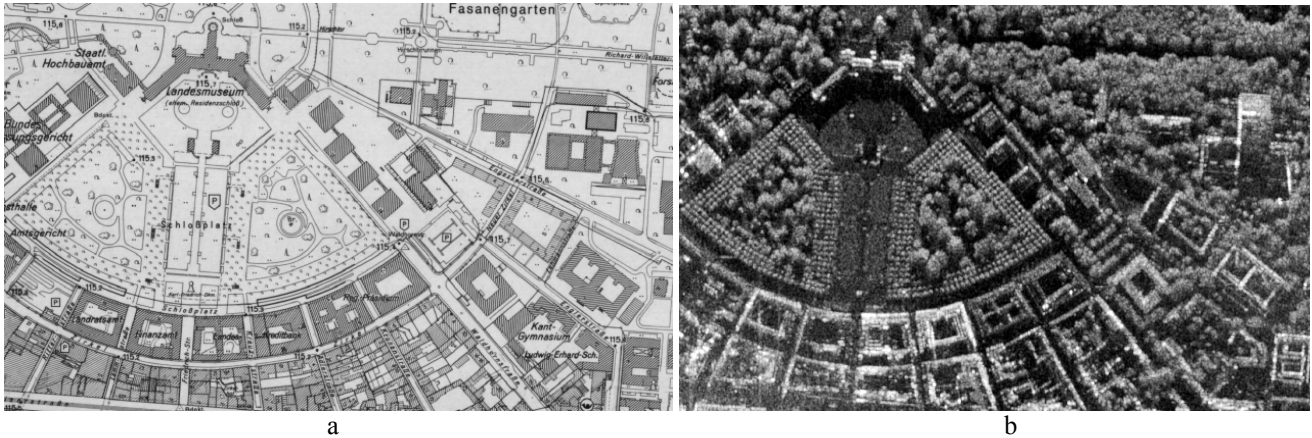


Fig. 1. a) Map section (DGK5, ©LBW) of test area Karlsruhe, Germany, and b) SAR image (1 pixel = 1m x 1m).

2. Elevation data from radar

2.1 Acquisition of SAR data

The moving sensor illuminates the scene with microwaves in a side-looking manner. The signal is partly either reflected away from the sensor or scattered towards the sensor, depending on the roughness of the scene compared to the signal wavelength. Hence, the choice of the sensor wavelength (e.g. X-band: 3cm, P-band: 64cm) depends on the task. Our test data were acquired with the airborne AER-II sensor of FGAN [Ender, 1998]. AER-II is equipped with an active, fully polarimetric phased array and uses a center frequency of 10 GHz (X-band). The bandwidth is 160 MHz. Four channels are available to record simultaneously the polarimetric combinations (HH, HV, VV, VH) or two interferograms (e.g. HH and HV).

2.2 Interferometric SAR principle

SAR interferometry takes benefit from the coherent SAR measurement principle. Fig. 2 illustrates the principle of airborne single-pass across-track interferometry measurement. Two antennas are mounted above each other on the carrier with geometric displacement B . One of the antennas illuminates the scene and both antennas receive the backscattered complex signals.

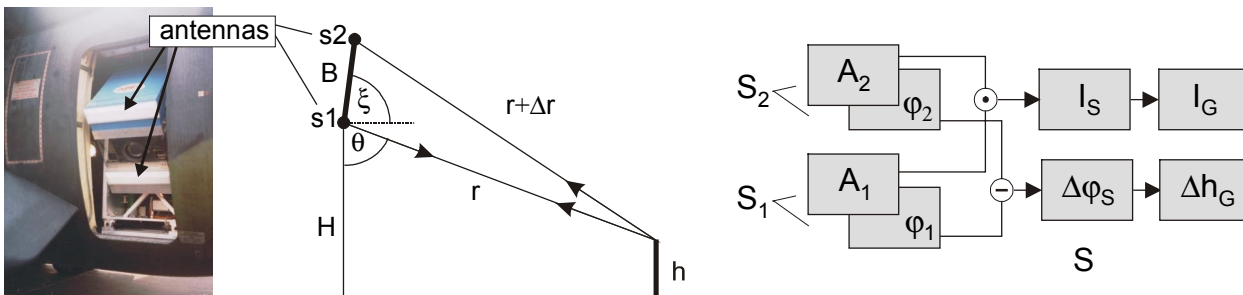


Fig. 2. SAR system AER II, geometry of across-track interferometry, and signal processing.

The interferogram S is calculated by a pixel by pixel complex multiplication of the master signal s_1 with the complex conjugated slave signal s_2 . Due to the baseline B , the distances from the antennas to the scene differ by Δr , which results in a phase difference $\Delta\phi$ in the interferogram:

$$S = s_1 \cdot s_2^* = a_1 \cdot e^{j\phi_1} \cdot a_2 \cdot e^{-j\phi_2} = a_1 \cdot a_2 \cdot e^{j\Delta\phi} \quad \text{with} \quad \Delta\phi = -\frac{2\pi}{\lambda} \Delta r \quad (1)$$

The phase difference $\Delta\phi$ is unambiguous in the range $]-\pi, \pi]$ only. Thus, a phase-unwrapping step is often required before further process. Furthermore, the range dependency of $\Delta\phi$ (Fig. 3b) has to be removed (flat earth correction). Afterwards, the elevation differences Δh in the scene can be derived from $\Delta\phi$:

$$\Delta h \approx \frac{\lambda}{2\pi} \cdot \frac{r \cdot \sin(\theta)}{B \cdot \cos(\xi - \theta)} \cdot \Delta\phi, \quad (2)$$

with parameters distance r , wavelength λ , antenna geometry angle ξ and viewing angle θ (Fig. 3c). The coherence γ is a function of the noise impact of the interferogram. It is usually estimated from the data by the magnitude of the complex cross-correlation coefficient of the SAR images:

$$\hat{\gamma} = \left| \frac{\sum_{n=1}^N s_1^{(n)} \cdot s_2^{(n)*}}{\sqrt{\sum_{n=1}^N |s_1^{(n)}|^2 \cdot \sum_{n=1}^N |s_2^{(n)}|^2}} \right| \approx 1 / \left(1 + \frac{1}{SNR} \right) \quad (5)$$

Hence, the local quality of an InSAR DEM can be directly assessed from the data by the related coherence value (Fig. 3d).

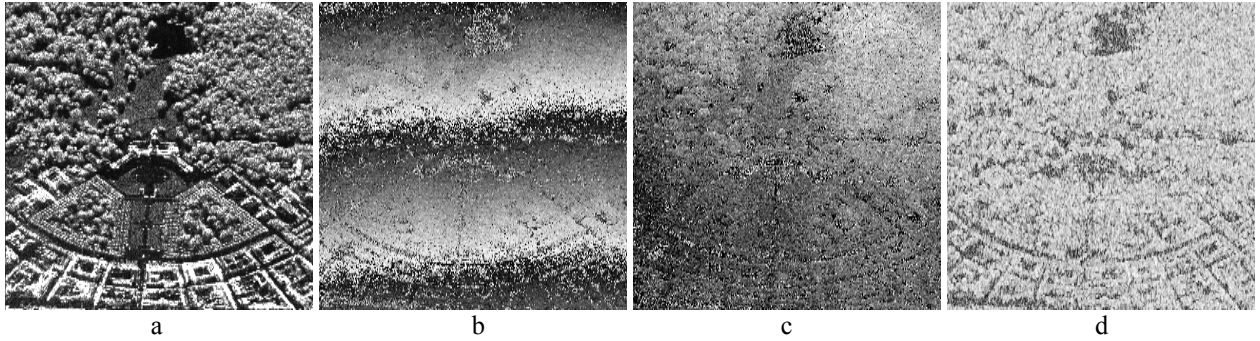


Fig. 3. Slant image (test area Karlsruhe). a) intensity, b) phase difference, c) elevation, d) coherence,

2.3 Geometric interpretation

Particularly in urban areas, phenomena like layover, shadow, multi-path signals and speckle [Schreier, 1993] have to be considered. Some of the phenomena are illustrated in Fig. 4. Let us assume that a building is sensed in a side looking manner from point F . In the slant range image I_S the points A, B, C appear according to their distance (Fig. 4a). Hence, the point A of the building footprint appears as A' behind point B' and in-between B' and C' . The area $B'A'$ is called layover area. Layover occurs always at vertical building walls facing towards the sensor. It leads to a mixture of signal contributions from the building and the ground in the SAR image, because the elevated objects are closer to the sensor than the ground. The slant image (see Fig. 3a) shows a geometric distortion in range direction which makes an object recognition and interpretation more difficult. Hence, for image interpretation the data are sampled to a rectangular grid on the ground (Fig. 4b). However, the order of the points B'', A'', C'' in the ground image is still the same as in the slant image. On the other side the building casts a shadow which occludes smaller objects behind and appears dark in the image. However, the height of a detached building can be derived from the shadow length and the viewing angle.

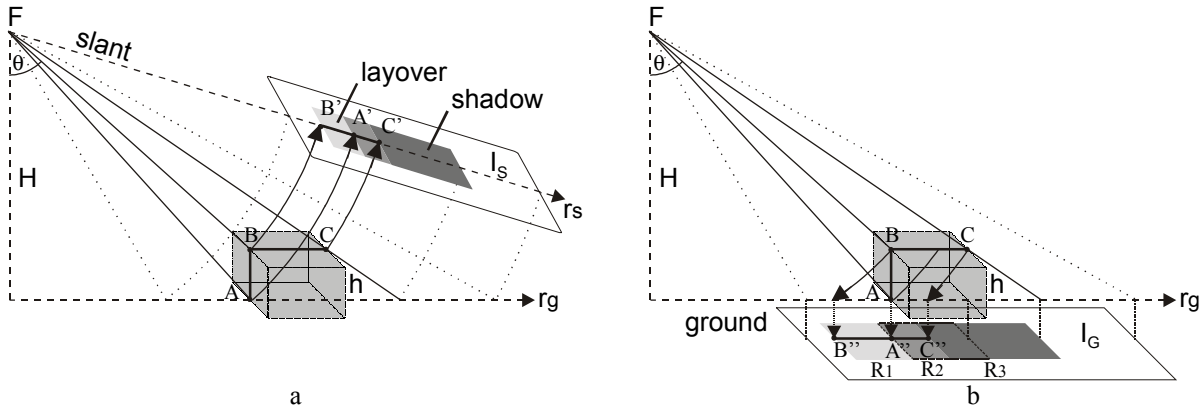


Fig. 4. Projection of a building into a) slant image (I_S) and b) ground image (I_G).

3. Segmentation of InSAR data

In our approach the entire set of complex InSAR data (phase, intensity, and coherence) is analyzed for the segmentation of extended buildings. An overview of the segmentation process is given in Fig. 5. In a pre-processing step the intensity data is despeckled and the elevation information is smoothed by median filtering. Fig. 5 (left, top) shows the intensity image (ground range) of a scene section of Frankfurt airport. The range direction is from top to down, ground resolution is approximately one meter. Corresponding to this image the elevation and coherence is shown. Several extended buildings are present in the scene at the airport Frankfurt. The rooftops are generally flat with small elevated superstructures, mostly required for illumination and air-conditioning inside the building.

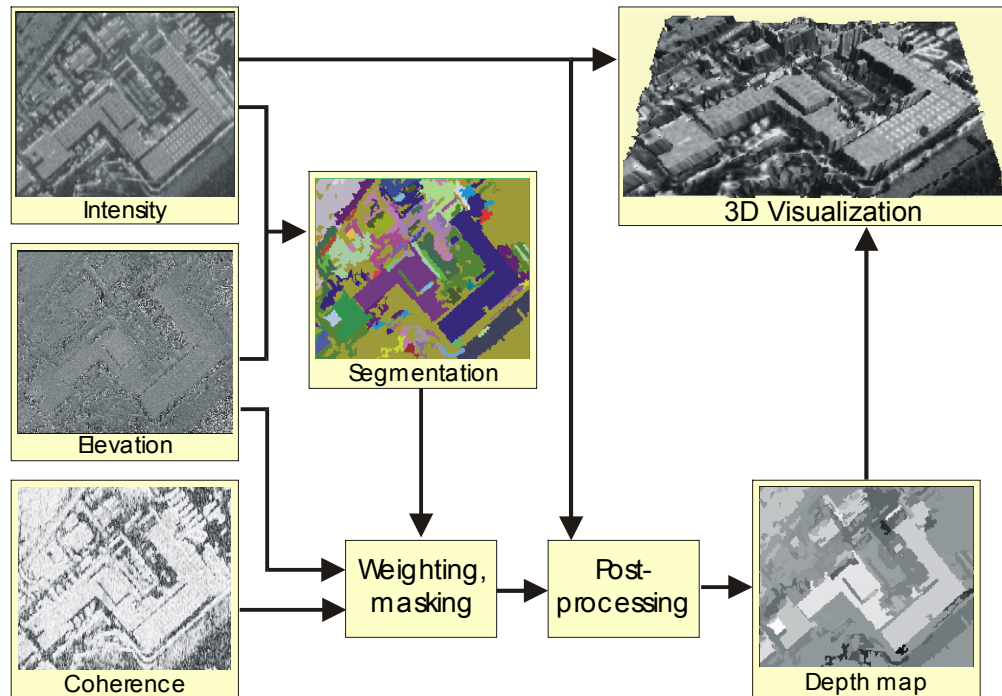


Fig. 5. Processing chain of the segmentation

3.1 Generation of a depth map considering the SNR

The initial segmentation is carried out by a combined region growing in the intensity and the elevation data [Soergel et al., 2000]. The threshold of region growing is set to a small value in order to detect as many object boundaries as possible. As a consequence, over-segmentation occurs, which is corrected in a subsequent post-processing step. In case of flat roof

structures and a constant SNR in the scene the average elevation of the roof is the MLE (maximum likelihood estimation) of the height measurements of the building. But the SNR varies in the scene. In order to consider this variation the elevation samples are weighted with the coherence for the averaging step. This results in a preliminary depth map of prismatic objects. Segments with low average intensity and coherence are regarded as unreliable. These segments are assumed to coincide with shadow areas or roads and are considered later to check the consistency of the results.

3.2 Detection of buildings

Elevated segments which match a building model according to size and shape are considered as building candidates. Shadow cast from a rectangular building part leads to either long or L-shaped segments, depending on the aspect. Their width is a function of viewing angle and object elevation. Hence, for each building candidate an expectation area for a shadow stripe is predictable. Unfortunately, shadow cannot always be distinguished from objects which appear similar in the data, like roads. Therefore, as a minimum requirement, an area of the set of unreliable segments is expected to be found at the predicted shadow location. If so, the candidate segment is labeled to be a building. In case shadow does not interfere with roads, a more subtle analysis is carried out. Shadow stripes are extracted in the intensity data with a simple structural image analysis algorithm.

3.3 Post-processing

Shadow areas are used to overcome under-segmentation. Segments which contain a possible shadow area are further investigated [Soergel et al., 2000]. The under-segmentation is corrected in two different ways. If the histogram of the original height values shows a bimodal curve, the segment is split in two closed segments, if possible. In a second approach a region growing step in the median filtered heights is performed. In contrast to the initial segmentation, the border towards the shadow region is used as seed [Hoepfner, 1999] and the threshold is smaller. Over-segmentation is corrected by merging adjacent segments with similar heights. After post-processing the depth map is recalculated.

4. Discussion

It was shown that in InSAR data a segmentation of building structures is possible. The InSAR test dataset Frankfurt contained large and detached buildings with flat roofs. Extended building parts with different height could be distinguished by the segmentation approach. Due to the noisy nature of the InSAR elevation data, the achieved level of detail was not comparable with results from LIDAR [Stilla & Jurkiewicz, 1999],[Stilla et al., 2000].



Fig. 6. a) oblique view of the scene, b) SAR image (ground range), c) vertical view, d) SAR image overlaid with the layer BULDING of the vector map. Range direction from right to left

The smoothed InSAR elevation data can be used for change detection purposes, at least for extended buildings. But the results indicate that the approach is limited to coarse scene descriptions only. For image based detail analysis, like roof reconstruction, the data is still too inaccurate. If a further improvement of the accuracy is achievable more sophisticated object models become appropriate in the future. The segmentation results might be used to correct the geometric displacement of the buildings. Furthermore, they could be incorporated in a refined phase unwrapping step in which shadow and layover areas are masked.

The reconstruction of man-made objects in dense urban areas from SAR imagery is limited by inherent geometric constraints. The mentioned effects of layover and shadow (explained in Fig. 4) are visible in Fig. 6. A part of the scene which was mapped by the SAR image of Fig. 1b contains a high building (see Fig. 6a). The corresponding section of the SAR image was rotated by 90° and is displayed in Fig. 6b. (Illuminated from right to left). For comparison a nadir view of the scene section is shown by an aerial image in Fig. 6c and the building layer of a digital vector map is overlaid (Fig. 6d). Due to the elevation the building appears shifted towards the sensor, covering partly a smaller building. Additionally, a building is partly occluded from the shadow cast by the high building.

As shown in Fig. 2b, layover (Area R1) leads to a signal mixture from ground and building (wall and roof), in contrast to area R2, which originates from the roof only. The width (A"C") of area R2 depends on angle θ and the building geometry w and h . R2 disappears if $h = w \tan \theta$ when the point C falls together with point A on the ground (Fig. 7a). That means, if $h = w \tan \theta$ a proper roof reconstruction is not possible anymore. As a consequence, for building reconstruction a large viewing angle θ is advantageous. However, a large θ leads to extended shadow regions behind buildings, which might occlude a lower building or street of width $s = h \tan \theta$ (Fig. 7b). Furthermore, the area of unreliable image data may be extended from layover l caused by buildings located at the other side of the street, as depicted in Fig. 7c.

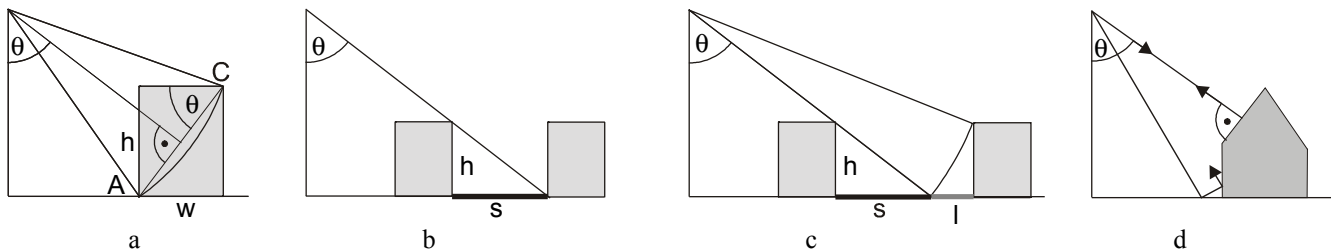


Fig. 7. Geometric constraints for the acquisition of SAR images from buildings.

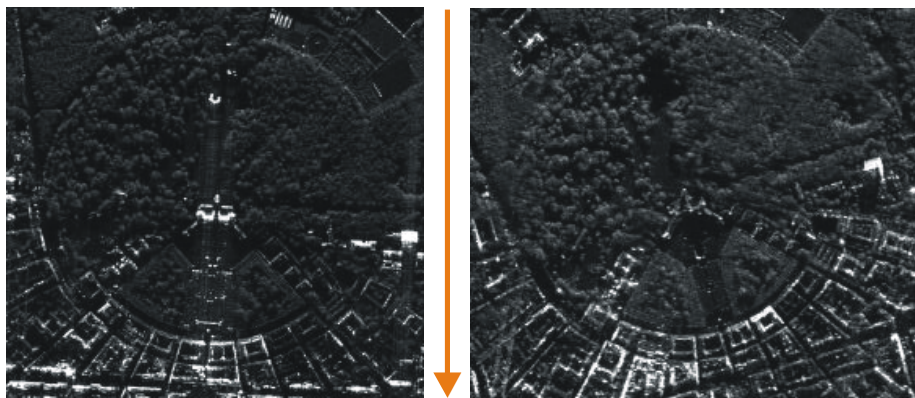


Fig. 8. Two SAR images taken from different flight paths. The arrow shows the range direction. The set of buildings (segment of the circle) which shows strong reflections differs in both images.

Additionally, roofs with perpendicular orientation towards the sensor cause total reflections and strong signal responses (Fig. 7d). Corners, antennas and sloped rooftops may lead to dominant scattering due to multi-bounce effects, respectively perpendicular orientation towards the sensor, depending on the aspect (e.g. at the circle around the castle in Fig. 8). At building walls multi-path propagation of signals occurs, which leads to a wrong range. Double-bounce propagation at the

extended dihedral corner reflector between the ground and the building wall is mapped to the location at the building footprint. This leads to a line of bright intensity in azimuth direction at the edge of the building wall and ground.

Because of the phenomena mentioned above the radar illumination aspect is important. Hence, the data acquisition of certain areas of the urban scene may be optimized by a simulation of SAR phenomena [Meier et al., 1993]. A suitable basis for such a simulation is a 3D city model, which can be obtained from LIDAR data [Soergel et al., 2002].

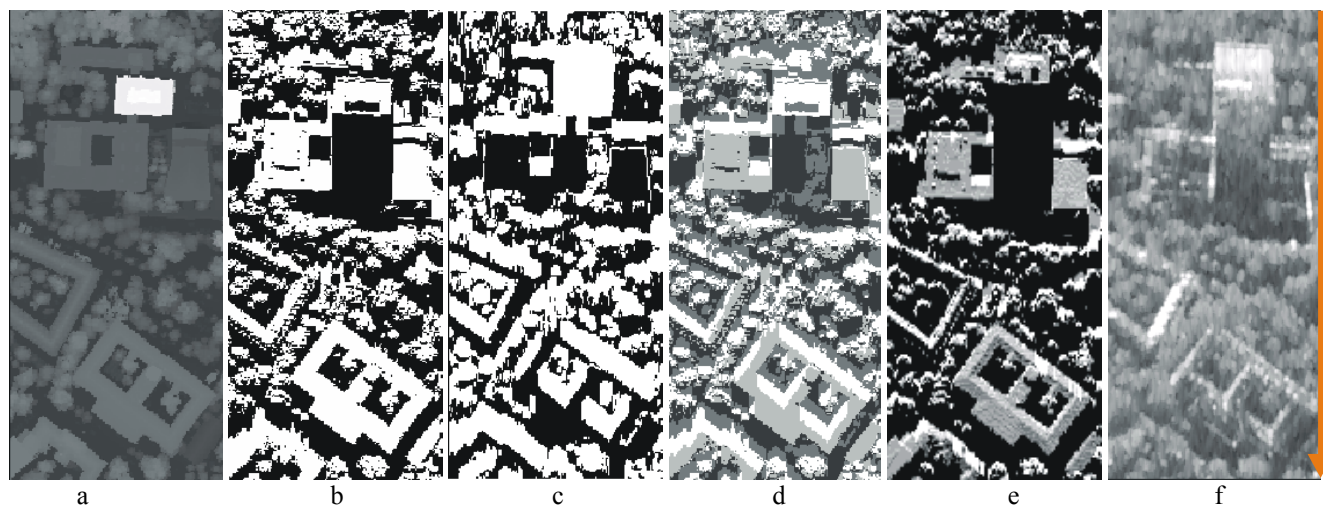


Fig. 9. a) Laser elevation data, b) shadow simulation, c) layover simulation, d) SAR phenomena image with shadow and layover, e) Simulation of SAR image, f) SAR image

In Fig. 9a such LIDAR data of a corresponding section of the test area Karlsruhe (University campus) is shown. The DEM is incorporated to predict geometric phenomena for an illumination from above with a view angle (off nadir angle) $\theta=55^\circ$. The calculated shadow areas are shown in Fig. 9b in black and layover areas are shown in Fig. 9c in white. A combined visualization of both effects is shown in Fig 9d. Layover is depicted in white, shadow in black, and areas with a mixture of layover and shadow appear dark gray. The region of the scenes which is expected to lead to undisturbed signal is shown in bright gray. A simple simulation of the SAR image is shown in Fig. 9e. The terrain slope is considered by weighting the contribution from the scene to each range bin according to a cosine model. In Fig. 9f the corresponding section of the SAR image which was acquired from the simulated position is depicted for comparison.

Acknowledgment

We want to thank Dr. Ender (FGAN-FHR Research Institute for High Frequency Physics and Radar Techniques) for providing us the InSAR data (AER II).

References

- Armbruster W, Bers KH (1998) Three-dimensional obstacle classification in laser range data. In: Andersen BF, Strojnik M (eds) IR technology and applications XXIV. SPIE conference on aerospace/defence sensing, San Diego, USA, Vol. 3436, 475-483
- Bolter R, Leberl F (2000) Phenomenology-based and interferometry-guided building reconstruction from multiple SAR images. Proc. EUSAR, 687-690
- Ender JHG (1998) Experimental results achieved with the airborne multi-channel SAR system AER-II. Proc. EUSAR'98, 315-318
- Gamba P, Houshmand, B (2000) Digital surface models and building extraction: A comparison of IF-SAR and LIDAR data. IEEE Trans. on Geoscience and Remote Sensing 38(4): 1959-1968

- Hoepfner KB (1999) Recovery of Building Structure from IFSAR-Derived Elevation Maps. Technical Report 99-16, Computer Science Department, University of Massachusetts, Amherst
- Kakumoto S, Hatayama M, Kameda H, Taniguchi T (1997) Development of disaster management spatial information system. Proc. GIS'97 Conf., 595-598
- Leberl KW, Bolter R (2001) Building reconstruction from Synthetic Aperture Radar images and interferometry. In: Baltsavias EP, Gruen A, VanGool L (eds) Automatic extraction of man-made objects from aerial and space images (III), 281-289. Lisse: Balkema
- Lee JS, Hoppel KW, Munge SA, Miller AR (1994) Intensity and Phase Statistics of Multilook Polarimetric and Interferometric SAR Imagery. IEEE Trans. on Geoscience and Remote Sensing 32(5): 1017-1028
- Meier E, Frei U, Nuesch D (1993) Precise terrain corrected geocoded images. In G. Schreier (ed) SAR Geocoding: Data and Systems: 173-185. Karlsruhe: Wichmann
- Meyer RH, Roy RJ (2000) Algorithms for interpreting SAR imagery of complex building scenes. In: Zelnio E (ed), Algorithms for synthetic aperture radar imagery VII, SPIE Proc. vol. 4053, 642-651
- Michaelsen E, Soergel U, Stilla U (2002) Grouping strong coherent scatterers for large building recognition in IFSAR data. Proc. ICPR 2002, (in press)
- Schreier G (1993) Geometrical properties of SAR images. In: Schreier G(ed) SAR geocoding: data and systems: 103-134. Karlsruhe: Wichmann
- Slatton KC, Crawford MM, Evans BL (2000) Combining interferometric radar and laser altimeter data to improve estimates of topography. Proc. IGARSS 2000 (on CD ROM)
- Soergel U, Thoennessen U, Gross H, Stilla U (2000) Segmentation of interferometric SAR data for building detection. International Archives of Photogrammetry and Remote Sensing, vol. 33, part B1, 328-335
- Soergel U, Schulz K, Thoennessen U, Stilla U (2002) Utilization of 2D and 3D information for SAR image analysis in dense urban areas. Proc EUSAR 2002 (in press)
- Stilla U, Jurkiewicz K (1999) Reconstruction of building models from maps and laser altimeter data. In: Agouris, P., Stefanidis, A. (eds.), Integrated spatial databases: Digital images and GIS: 34-46. Berlin: Springer
- Stilla U, Soergel U, Jaeger K (2000) Generation of 3D-city models and their utilisation in image sequences. International Archives of Photogrammetry and Remote Sensing, vol. 33, part B2, 518-524
- Takeuchi S, Suga Y, Yonezawa C, Chen CH (2000) Detection of urban disaster using InSAR - a case study for the 1999 great Taiwan earthquake. Proc. IGARSS 2000 (on CD ROM)
- Walesa M, Datcu M (2000) Enhancement of interferometric DEMs by spatially adaptive model-based filtering in non-stationary noise. Proc. EUSAR, 695-698
- ©LBW Permission granted by Landesvermessungsamt Baden-Württemberg, Aussenstelle Karlsruhe